Formationkeeping for a Pair of Satellites in a Circular Orbit

Richard H. Vassar* and Richard B. Sherwood†
TRW, Redondo Beach, California

Certain future missions will require that a pair of satellites—master and slave—fly in a fixed relative formation. Active control is required to maintain this formation in spite of disturbances such as aerodynamic drag and solar radiation pressure. This paper develops a closed-loop formationkeeping controller for satellites in any circular orbit using digital optimal control theory. A formationkeeping sensor concept, tradeoffs, design, brassboard demonstration, and modeling are discussed. The formationkeeping actuators are assumed to be chemical thrusters on the slave satellite. Two satellites flying in trail 700 m apart in geosynchronous orbit are used as an example to present closed-loop formationkeeping simulation plots. The results show that formation is maintained to within the ±21 m allocated requirement in the in-track and out-of-plane directions.

Nomenclature

$b_x, b_y, b_z, b_{\dot{x}}, b_{\dot{y}}, b_{\dot{z}}$ = biases in the measured slave position and position rate
C = sensor scale factor
CCD = charge coupled device
$\bar{f}$ = disturbance specific force, i.e., difference between the specific force acting on the slave and the specific force acting on the master
f_x, f_y, f_z = components of $\bar{f}$ in the $\hat{x},\hat{y},\hat{z}$ coordinate frame
f_1, f_2, f_3 = components of $\bar{f}$ in the inertial coordinate frame parallel to $\hat{x},\hat{y},\hat{z}$ at time zero
LEPD = lateral effect photodiode
master = reference satellite
P = orbit period
$r_x, r_y, r_z, r_{\dot{x}}, r_{\dot{y}}, r_{\dot{z}}$ = random noise in the measured slave position and position rate
slave = satellite whose position is controlled relative to the master
T = sample rate, e.g., time between thruster firings
x,y,z = slave satellite position coordinates in the $\hat{x},\hat{y},\hat{z}$ coordinate frame
$\dot{x},\dot{y},\dot{z}$ = time derivative of x,y,z taken in the $\hat{x},\hat{y},\hat{z}$ coordinate frame
x_k, y_k, z_k = x,y,z at time t_k
$x_{k+1}, y_{k+1}, z_{k+1}$ = x,y,z at time $t_{k+1} = t_k + T$
x_m, y_m, z_m = measured slave position in the $\hat{x},\hat{y},\hat{z}$ coordinate frame
$\hat{x},\hat{y},\hat{z}$ = unit vectors in the Earth-pointing coordinate system with master at the origin; $\hat{x}$ is along the velocity vector, $\hat{y}$ is antiparallel to the orbital angular momentum, and $\hat{z}$ points toward nadir
$\Delta V_{x_k}, \Delta V_{y_k}, \Delta V_{z_k}$ = components of the impulsive velocity change at time t_k in the $\hat{x},\hat{y},\hat{z}$ coordinate frame
θ = orbit angle measured from the first point of Aries ($i = 0$)
ω_0 = orbit rate

Received Aug. 11, 1983, revision received March 28, 1984.

*Member of the Technical Staff; currently Associate Scientist—Research, Lockheed Palo Alto Research Laboratory, Palo Alto, Calif. Member AIAA.

†Staff Engineer, Control and Sensor Systems Laboratory. Member AIAA.

Introduction

UNLIKE stationkeeping, where a satellite's position is controlled relative to its subsatellite point, formationkeeping involves the control of one or more satellites relative to another satellite.

A demonstration of formationkeeping occurred in mid-June 1983 during Shuttle mission 7.[1] The Shuttle under astronaut manual control flew in formation with the SPAS satellite to demonstate the Shuttle's ability to deploy and retrieve satellites using the remote manipulator arm. In the future formationkeeping will be more common and more automatic. The Shuttle/SPAS mission was an example of an observation spacecraft that maneuvers to and operates in the vicinity of another spacecraft. Another formationkeeping application is a materials processing satellite carried into space by the Shuttle. In order to perform sensitive materials processing in a low g environment, the satellite is separated from the Shuttle but remains nearby to facilitate transfer of raw materials and finished products. The last example is a ground-based terrestrial laser communication system. A laser beam originating from a ground station is bounced off a mirror on a master satellite in geosynchronous orbit to a receiver at a second ground station many miles from the transmitter (similar to Echo, the pioneer radio communication satellite). To limit power losses in the uplink laser beam to an acceptable level, it is necessary to calibrate the beam's path through the atmosphere by a small probe laser illuminating the ground station from a slave satellite that remains a fixed distance ahead of the master satellite in orbit.

This paper develops a practical control scheme, applicable to any circular orbit, whereby a satellite can fly in formation with another satellite. First, the optimal control algorithms are developed. An optical sensor applicable to the formationkeeping control is described and modeled. Closed-loop performance results are presented for a geosynchronous trail satellite geometry exemplified by the laser communication system. Finally, some conclusions derived from the study are summarized.

Orbital Dynamics

The motion of one satellite with respect to another in a circular or near-circular orbit (see Appendix for derivation) can be analyzed using the Clohessey-Wiltshire equations, a linearized set of orbit equations. Siefert[2] and Clohessey and Wiltshire[3] were the first to use these equations to analyze the motion of one satellite in the vicinity of another. Figure 1 shows the coordinate system used, where $\hat{x}$ is along the velocity vector, $\hat{y}$ is perpendicular to the orbit plane in the

opposite sense of the angular momentum vector, and $\hat{z}$ is directed toward nadir. The Clohessey-Wiltshire equations (also sometimes called Hill's equations) in this coordinate system are

$$\ddot{x}=2\omega_0\dot{z}+f_x$$

$$\ddot{y}=-\omega_0^2 y+f_y$$

$$\ddot{z}=-2\omega_0\dot{x}+3\omega_0^2 z+f_z \tag{1}$$

where x, y, z is the position of the slave satellite in the $\hat{x}$, $\hat{y}$, $\hat{z}$ frame with the master satellite at the origin, ω_0 the orbit rate, and f_x, f_y, and f_z components of $\bar{f}=\bar{f}_{\text{slave}}-\bar{f}_{\text{master}}$. These equations show that the out-of-plane and in-plane motions are decoupled. The out-of-plane motion is equivalent to the motion of a mass on a massless spring with eigenvalues at $\pm\omega_0 j$. The eigenvalues of the in-plane system are 0, 0, $\pm\omega_0 j$. The associated modes are a constant separation in the $\hat{x}$ direction, a constant velocity in the $\hat{x}$ drection, and motion of one satellite about the other (due to small differences in eccentricity).

The uncontrolled response depends on the disturbance $\bar{f}$. The disturbance is determined by environmental factors such as solar pressure, air drag, or gravitational perturbations and the physical characteristics of the two satellites. If, for example, both satellites are spheres with different densities but equal reflectivities, then the resulting disturbance $\bar{f}$ due to solar radiation pressure is constant in inertial space. When $\bar{f}$ is expressed in the $\hat{x}$, $\hat{y}$, $\hat{z}$ coordinate system, the f_y component is constant but the f_x and f_z components are sinusoidal at orbit rate. The constant out-of-plane disturbances results in displaced undamped oscillatory motion of the slave relative to the master. As stated above, the in-plane equations exhibit an undamped mode at orbit rate. The equations are forced at that frequency by differential solar radiation pressure; hence, the in-plane relative position grows without bound until the linearized equations (1), no longer apply.

Lange[4] determined the exact analytical solution to Eq. (1) for an inertially constant disturbance $\bar{f}$. The solution, for $x_0=y_0=z_0=\dot{x}_0=\dot{y}_0=\dot{z}_0=0$, is

$$x=\frac{f_1}{\omega_0^2}\left[3\omega_0 t\sin\omega_0 t-5(1-\cos\omega_0 t)\right]$$

$$-\frac{f_3}{\omega_0^2}\left[3\omega_0 t-6\sin\omega_0 t+3\omega_0 t\cos\omega_0 t\right]$$

$$y=\frac{f_2}{\omega_0^2}(1-\cos\omega_0 t)$$

$$z=-\frac{3}{2}\frac{f_1}{\omega_0^2}\left[\sin\omega_0 t-\omega_0 t\cos\omega_0 t\right]$$

$$+\frac{f_3}{\omega_0^2}\left[\frac{3}{2}\omega_0 t\sin\omega_0 t-2(1-\cos\omega_0 t)\right] \tag{2}$$

where f_1, f_2, and f_3 are the components of $\bar{f}$ along the $\hat{x}$, $\hat{y}$, and $\hat{z}$ axes at $t=0$. Equation (2) shows the behavior argued on physical principals in the previous paragraphs, that is, that y is displaced undamped oscillatory motion and x and z grow without bound.

Figure 2 shows the uncontrolled in-plane response, obtained by numerically integrating Eq. (1) using a Fourier series model of the actual solar pressure forces for the two satellites of the laser communication example. The actual solar pressure force magnitude and direction in inertial space varies slightly with the orbit angle. This simulation result, for "real" satellites, shows the same behavior as the analytic results for the spherical satellites, i.e., unbounded in-plane error growth over time. Clearly, this is unacceptable since the objective is to maintain the in-track position within the bounds dictated by mission requirements. Hence, some type of disturbance compensation scheme is required.

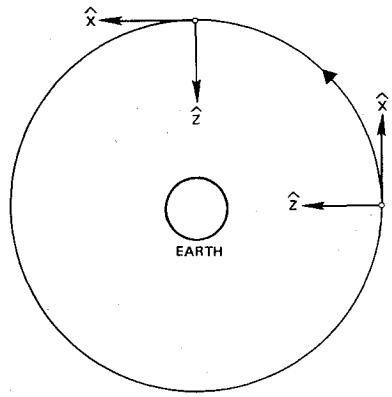

Fig. 1 Coordinate system.

Controller Design

One way to cancel the disturbance $\bar{f}$ is to operate thrusters on one of the satellites. Since chemical thrusters, being on/off devices, cannot be operated in a continuous proportional manner, digital (or discrete) control is a natural solution. Most of the disturbance can be cancelled by following a predetermined open-loop thruster profile based on a priori estimates of the disturbance. A simple open-loop thruster profile is obtained by differencing the expected solar pressure specific forces acting on the satellites and multiplying by the time between thruster firings. This is approximately the relative velocity that accumulates between thruster firings. The negative of this is the simple open-loop ΔV. Because of modeling errors, this compensation scheme will not achieve perfect cancellation and the satellites will slowly drift from their desired positions, eventually exceeding the error bound. However, a properly designed closed-loop controller will stabilize the system and keep the error small.

Another approach is to adjust the reflectivities on the two satellites until the disturbance $\bar{f}$ is zero. However, this is impractical for several reasons: reflectivities are chosen on the basis of a thermal design and therefore are not free to be specified by the formationkeeping engineer and even if this were not the case it would be difficult to vary the reflectivities on orbit (for closed-loop control) in response to changes in the disturbance.

Thus, two candidate formationkeeping schemes, both of which use thrusters as actuators, are: 1) a closed-loop controller or 2) an open-loop thruster profile and a closed-loop controller. The remainder of this paper will focus on scheme 1. Qualitative results for scheme 2 are discussed briefly in the conclusions.

Bryson[5] has developed bang-bang, bang-off-bang, and optimal continuous controllers for stationkeeping. This paper will extend these results by developing optimal digital controllers for formationkeeping. Taking advantage of the decoupling in the Clohessey-Wiltshire equations, the controllers for the in-plane and out-of-plane problems are designed separately. The in-plane control problem is multi-input, multi-output with two actuators, thrust in the $\hat{x}$ and $\hat{z}$ directions, and two responses x and z. The system, being highly coupled, cannot be broken into separate single-input, single-output systems and hence does not lend itself to analysis using classical control techniques. Optimal control theory with a quadratic cost function offers a simple solution. The usual reservations with using optimal control theory for practical designs (i.e., uncertainty in the system parameter values) do not apply to this problem because the plant

parameter, i.e., orbit rate, is known accurately and is essentially constant.

The following cost function was used for the in-plane problem (position error in the z direction was not included in the cost function because the terrestrial laser communication system performance is insensitive to slave position error in the $\hat{z}$ direction):

$$J=\frac{1}{2}\sum_{k=1}^{\infty}\left[x_k^2+\left(\frac{\Delta V_{x_k}}{\omega_0}\right)^2+\left(\frac{\Delta V_{z_k}}{\omega_0}\right)^2\right] \tag{3}$$

For a digital controller the sample time or time between thruster firings must be selected. Two conflicting objectives define a tradeoff on thruster firing frequency: 1) minimizing in-track position error implies frequent corrections and 2) minimizing disturbances to spacecraft and minimizing the controller computational burden implies that the time between formationkeeping corrections should be long. A value of, $T=P/24$ (i.e., 1 h in geosynchronous orbit) was selected as the time between thruster firings (see Fig. 13 and discussion in the section on simulation results).

The discrete in-plane state equations are (where time has been normalized by $1/\omega_0$)

$$\begin{bmatrix}\dot{x}_{k+1}\\ x_{k+1}\\ \dot{z}_{k+1}\\ z_{k+1}\end{bmatrix}=\begin{bmatrix}0.863 & 0 & 0.519 & 0.206\\ 0.250 & 1 & 0.0685 & 0.0180\\ 0.519 & 0 & 0.966 & 0.778\\ -0.0685 & 0 & 0.259 & 1.10\end{bmatrix}\begin{bmatrix}\dot{x}_k\\ x_k\\ \dot{z}_k\\ z_k\end{bmatrix}$$

$$+\begin{bmatrix}0.863 & 0.519\\ 0.250 & 0.0685\\ -0.519 & 0.966\\ -0.0685 & 0.259\end{bmatrix}\begin{bmatrix}\Delta V_{x_k}\\ \Delta V_{z_k}\end{bmatrix} \tag{4}$$

The steady-state in-plane control laws obtained by solving the discrete matrix Ricatti equation[6-9] are

$$\Delta V_{x_k}=-0.456\dot{x}_k-0.454\omega_0 x_k+0.0197\dot{z}_k+0.458\omega_0 z_k$$

$$\Delta V_{z_k}=0.0197\dot{x}_k-0.547\omega_0 x_k-0.546\dot{z}_k-0.868\omega_0 z_k \tag{5}$$

The in-plane closed-loop roots are shown in Table 1. The control law is general for any near-circular orbit. Just substitute the appropriate value for the orbit rate ω_0.

The same approach was applied to the out-of-plane problem using the following cost function:

$$J=\frac{1}{2}\sum_{k=1}^{\infty}\left[y_k^2+\left(\frac{\Delta V_{y_k}}{\omega_0}\right)^2\right] \tag{6}$$

Because out-of-plane control is much less demanding than in-plane control, $T=P/6$ was selected as the time between out-of-plane formationkeeping ΔV. The discrete out-of-plane state equations for this sample rate are (where time has been normalized by $1/\omega_0$)

$$\begin{bmatrix}\dot{y}_{k+1}\\ y_{k+1}\end{bmatrix}=\begin{bmatrix}0.498 & -0.867\\ 0.867 & 0.498\end{bmatrix}\begin{bmatrix}\dot{y}_k\\ y_k\end{bmatrix}+\begin{bmatrix}0.498\\ 0.867\end{bmatrix}\Delta V_{y_k} \tag{7}$$

The steady-state out-of-plane control law obtained by solving the discrete matrix Riccati equation is

$$\Delta V_{yk}=-0.608\dot{y}_k-0.152\omega_0 y_k \tag{8}$$

The out-of-plane closed-loop roots are shown in Table 1. The control law is general for any near-circular orbit. Just substitute the appropriate value for orbit rate ω_0.

Example

Description

Formationkeeping controller performance will be demonstrated for the terrestrial laser communication system. A mirror is carried on the master satellite in geosynchronous orbit. A communication laser beam originating from a ground station is bounced by the mirror to another ground station many miles away. To keep the laser uplink from being dispersed as it passes through the atmosphere, a slave satellite must lead the master satellite in orbit so that its small laser can calibrate a column of air for the uplink. The proper lead distance is approximately the round-trip travel time of light to the geosynchronous altitude times the orbital velocity of the satellite. For effective calibration (i.e., to reduce the laser power loss to an acceptable level), the slave position, both in-track and out-of-plane, has been allocated a position error of 3% of the nominal 700 m range between the slave and master satellites. To first order, system performance is insensitive to position error along the $\hat{z}$ axis.

The example satellites have the characteristics shown in Table 2. Now a simple sensor for measuring slave satellite position relative to the master will be discussed.

Sensor Characteristics

The formationkeeping control system relies upon a sensor that can measure the three components of relative satellite position: range, cross-range, and elevation. Radar and laser rangefinders are available for this task; however, they exact a great penalty in complexity and weight in order to provide a high degree of measurement accuracy that is not warranted by this problem. The device employed in the foremationkeeping sensor system is a simple telescope that produces an image of the target upon a lateral-effect photodiode (LEPD), an analog detector whose differential current output is an accurate measure of the location of the image along its sensitive axis. A laser diode modulated at 200 Hz is used as the target to enable discrimination of interference sources and the elimination of bias via ac coupling. Two orthogonal detectors mounted on one satellite and a single target mounted on the other vehicle enable determination of the two cross-range components of

Table 1 Closed-loop roots

Roots[a]	ω	ζ
In-plane		
$0.61\pm0.38j$	2.5	0.5
0.62	1.8	
0.76	1.0	
Out-of-plane		
$0.28\pm0.56j$	1.14	0.39

[a] In z plane where time has been normalized by $1/\omega_0$.

Table 2 Slave and master satellite characteristic

	Slave satellite	Master satellite
Stabilization method	Dual spinner	3-axis
Weights, kg	410	1550
Dimensions, m		
Diameter	3.5	2.4
Length	0.5	1.3
Mirror diameter, m		7
Surface reflectivity	0.26	0.80

position. Two methods can be used to determine range. The first, designated stadiametric, employs two targets separated by a known baseline and modulated at different frequencies to enable their discrimination at the receiver. To first order, range is simply the known baseline divided by the apparent angle subtended by the targets at the receiver. Because target rotation can confuse the range determination by foreshortening the baseline, a third target is added, nominally perpendicular to the baseline and along the line of sight, to resolve the problem. The geometry is shown in Fig. 3. Note that target attitude is determined as a by-product of this arrangement.

The proliferation of targets in the stadiametric scheme leads to an alternative sensor configuration designated stereometric. Essentially a binocular sensor, this system uses an extra receiver but only one target. The baseline necessary for range determination is now between the two receivers and is colinear with their sensitive axes. The geometry, shown in Fig. 4, is the dual of the prior arrangement. The stereometric system is preferred for the system under study because the targets are mounted on the simpler, less stable slave satellite; their complexity, weight, and power consumption should be minimal. The receivers are mounted on the more stable master satellite so that apparent target motion due to receiver base motion uncertainty is minimized and advantage can be taken of the more extensive signal processing and base motion determination of the master satellite.

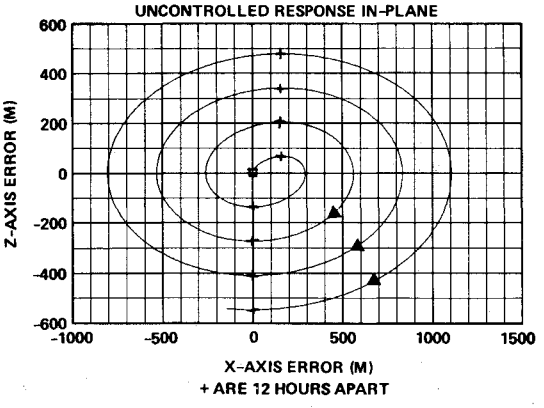

Fig. 2 Uncontrolled in-plane position of the slave satellite as seen from the master satellite.

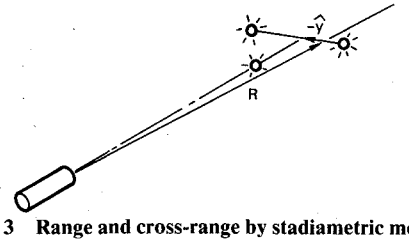

Fig. 3 Range and cross-range by stadiametric means.

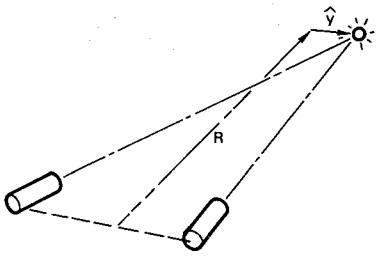

Fig. 4 Range and cross-range by stereometric means.

Figure 5 shows the device constructed and tested to demonstrate the requisite accuracy of the sensor system and to validate the sensor model employed in the formationkeeping simulations. Although a linear charge-coupled device (CCD) array might have been substituted for the lateral-effect photodiode, a tradeoff (Table 3) showed that the CCD requires larger optics, greater information processing bandwidth and is more susceptible to background interference.

The principal errors in the sensor system are noise, detector nonlinearity and receiver coalignment errors. Table 4 evaluates these sources for a system for three receivers mounted on a graphite epoxy spar, as shown in Fig. 6, to minimize misalignments. Also listed are the contributions from base motion uncertainties, assuming an Earth sensor measures satellite pitch and a star sensor measures yaw.

Figure 7 is a photograph of the receiver test installation used to confirm the design. The geometry of the range was scaled 1:100 to fit the available laboratory space, and the receiver baseline is only 2 cm. Ranging tests for co-orbital satellites yielded errors below 0.8 m when using a linear fit and scaling to operational size.

Nonlinear Simulation

A realistic nonlinear (inverse square gravitational field) simulation was developed to evaluate the closed-loop formationkeeping system performance for the terrestrial laser communication system. The simulation contained realistic models of the solar pressure disturbance, sensor, and thrusters.

The solar pressure specific force was calculated by modeling the satellite as a collection of plates and cylinders, each with its own reflectivity. A computer program was used to calculate the solar force vector at a number of points along the orbit. The program then fit a Fourier series in orbit angle θ to the data. The Fourier series model used in the simulation was truncated after the fifth harmonic, which introduced less

Table 3 Linear CCD and lateral effect photodiode detector comparison

Parameter	LCCD	LEPD
Number of cells	2048	1
Cell size	13×13 μm	1×6 mm
Active length, mm	26.6	6
Focal length, mm	300	50
Image quality	Diffraction limited	20× diffraction limited
Aperture	40 mm diam	20×20 mm
Signal-to-noise ratio	188	154,000
Noise equivalent angle, μ rad	0.23	0.39
Nonlinearity, μ rad	2.2	2.0
Sampling rate, Hz	819,000	800
Word length, bit	10	16
Three-sensor bit rate, bit/s	25×10^6	38×10^6

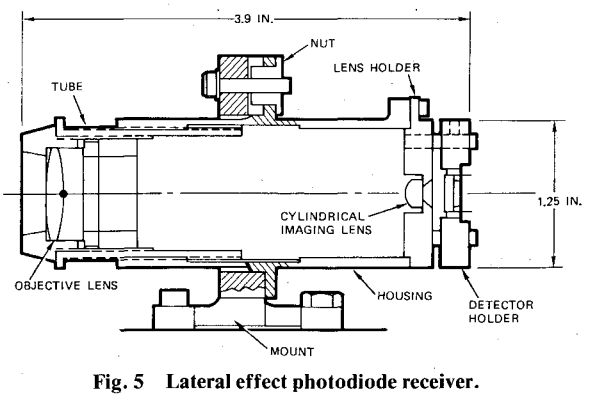

Fig. 5 Lateral effect photodiode receiver.

than a 1% error. As an example, the solar pressure specific force models used for summer solstice, beginning-of-life (BOL) were:

Slave

$$f_x = -4.66\times10^{-8}\cos\theta \text{ m/s}^2$$

$$f_y = 3.70\times10^{-8} \text{ m/s}^2$$

$$f_z = 4.66\times10^{-8}\sin\theta \text{ m/s}^2$$

Master

$$f_x = (-7.16\times10^{-8}\cos\theta + 2.79\times10^{-9}\cos 3\theta + 1.12\times10^{-9}\cos 5\theta - 4.43\times10^{-9}\sin 2\theta) \text{ m/s}^2$$

$$f_y = (2.19\times10^{-8} - 1.68\times10^{-9}\cos 2\theta - 7.41\times10^{-10}\cos 4\theta + 3.84\times10^{-9}\sin\theta) \text{m/s}^2$$

$$f_z = (-4.43\times10^{-9} + 4.43\times10^{-9}\cos 2\theta + 1.99\times10^{-7}\sin\theta - 2.79\times10^{-8}\sin 3\theta - 4.09\times10^{-9}\sin 5\theta) \text{m/s}^2$$

The slave satellite thruster configuration simulated in the study is shown in Fig. 8. This thruster configuration reduces the number of thrusters on the slave satellite over a more conventional arrangement. Notice that the in-plane thruster is canted 15 deg out-of-plane. To produce negative out-of-plane thrust the in-plane thrusters are fired together. The geometry necessitates an augmentation of the in-plane control logic described earlier. The in-plane logic directs the coordinated firing of the out-of-plane thruster to cancel the negative out-of-plane disturbances due to in-plane corrections. Each thruster produces 0.2 lb of force beginning-of-life, which drops to 0.1 lb at end-of-life. Because the hydrazine thrusters are operated in pulse mode, an I_{sp} of 150 s was assumed, as opposed to 200-210 s for continuous thrusting. Minimum thruster on-time is 20 ms. If a pulse smaller than 20 ms is specified by the control law, then the control logic does not command the thruster. Long in-plane thruster pulses are subdivided into several shorter pulses lasting 170 ms or less (during a 170 ms pulse the thrust vector will rotate 60 deg in inertial space due to the 1 rps spin rate) to maintain high thruster efficiency. The desired thrust direction is achieved by using a timer to operate the thruster; the timer is started by a sun detection pulse from the slit sun sensor.

The simulation sensor model is:

$$x_m = x + b_x + r_x$$

$$y_m = Cy + b_y + r_y$$

$$z_m = Cz + b_z + r_z$$

$$\dot{x}_m = \dot{x} + b_{\dot{x}} + r_{\dot{x}}$$

$$\dot{y}_m = C\dot{y} + b_{\dot{y}} + r_{\dot{y}}$$

$$\dot{z}_m = C\dot{z} + b_{\dot{z}} + r_{\dot{z}}$$

where x_m = measured x, x = true x, b_x = bias in measurement of x, r_x = random noise in measurement of x, and C = scale factor. Table 5 gives the values of bias b and noise r that were used in the simulation, based on the sensor error budget of Table 4. $C = x_m/x$ is the scale factor model.

Simulation Results

Simulation results are shown for the solar pressure disturbance given previously, including sensor noise and worst-case bias, without an open-loop thruster profile. In-plane error is shown in Fig. 9. The slave position is plotted looking down on the orbit plane from the north pole. The position is plotted for four orbits, with each cycle representing 24 h. The maximum in-track error is approximately 7.5 m, well within the requirement.

Out-of-plane position error is shown in Fig. 10. In this figure slave position is plotted relative to the master satellite looking edge on at the orbit plane. The maximum out-of-plane error is less than 5 m, again well within the ±21 m requirement.

Figure 11 shows the duration of the in-plane thruster control pulses. The longest pulses are less than half a second. The in-plane thruster activity will consume approximately 10 kg of hydrazine over the 8 yr worst case, with the satellite masses and thruster configurations assumed.

Figure 12 shows the duration of the out-of-plane control pulses, including those to cancel the out-of-plane thrust component of the canted in-plane thrusters. Most of the

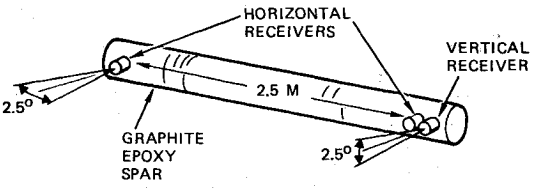

Fig. 6 Stereometric sensor system.

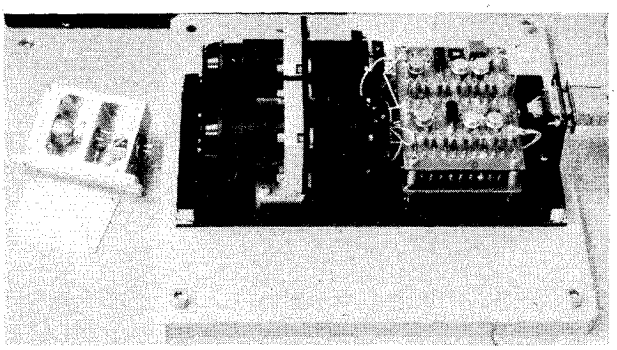

Fig. 7 Hardware for laboratory sensor test.

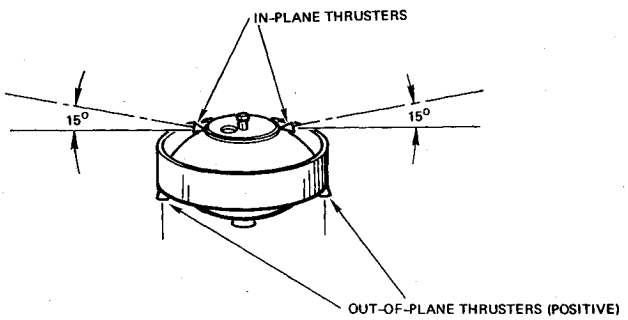

Fig. 8 Slave satellite thruster configuration.

Table 4 Sensor error budget (μrad)

x (range)	1 σ noise	1 (100 s averaging)
	Nonlinearity	2 (after cubic fit)
	Coalignment	1
y (out-of-plane)	Sensor	3
	Base motion	50 (10 arcsec star tracker)
z (altitude)	Sensor	3
	Base motion	350 (1 arc min Earth sensor)

pulses are cancellation pulses, with out-of-plane controller pulses occurring only every 4 h. The out-of-plane thruster will consume approximately 2.5 kg of propellant over the 8 yr worst case.

The total propellant consumed over 8 yr is about 12.5 kg (worst case) or approximately 3% of the slave satellite mass. This is small compared to the amount of propellant typically carried for attitude control and stationkeeping.

Optimal digital in-plane formationkeeping controllers were designed for several other sample rates, i.e., 30 min, 2 h, and 4 h. Simulation runs were made with each controller. Figure 13 is a plot of maximum in-track error as a function of the

Table 5 Simulation bias and random noise values

Parameter	b, worst case	r, 1σ
x	0.20 m	0.09 m
y	0.034 m	1.6×10-4 m
z	1.22 m	2.2×10-4 m
$\dot{x}$	0	3.9×10-5 m/s
$\dot{y}$	0	6.8×10-8 m/s
$\dot{z}$	0	9.6×10-8 m/s

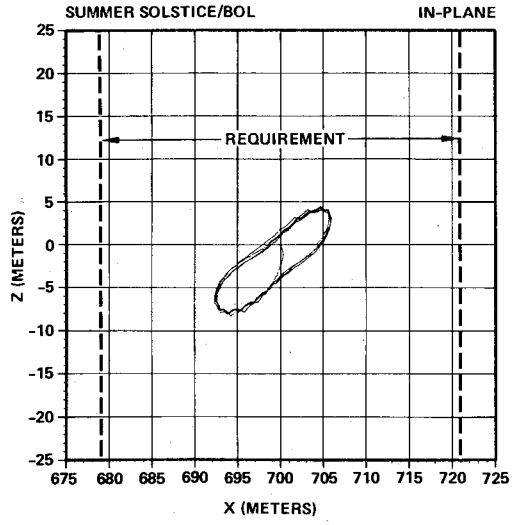

Fig. 9 In-plane slave satellite position during formationkeeping.

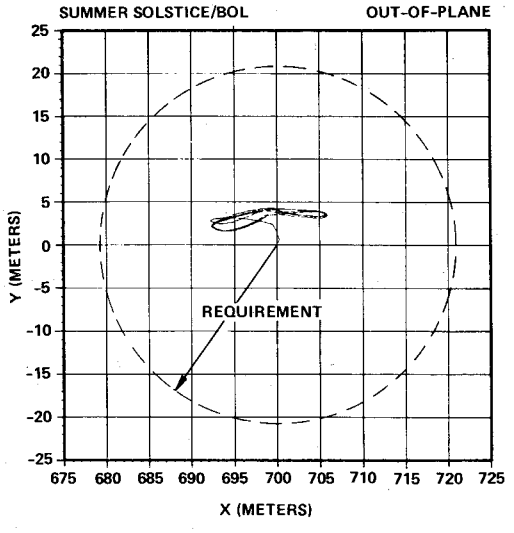

Fig. 10 Out-of-plane slave satellite position during formationkeeping.

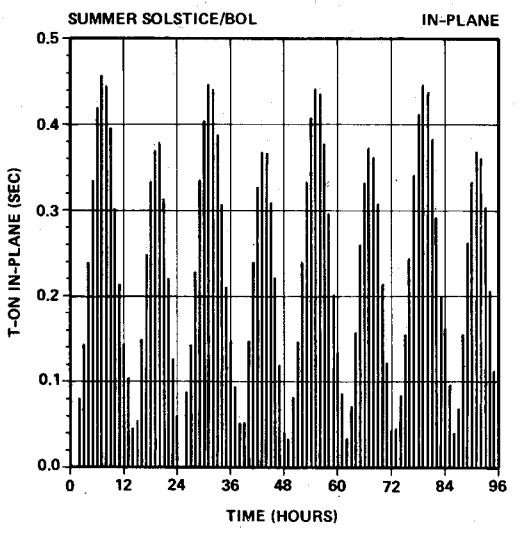

Fig. 11 In-plane formationkeeping thruster pulse duration.

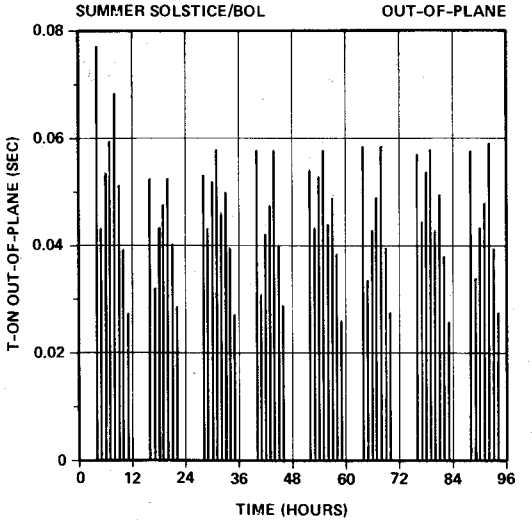

Fig. 12 Out-of-plane formationkeeping thruster pulse duration.

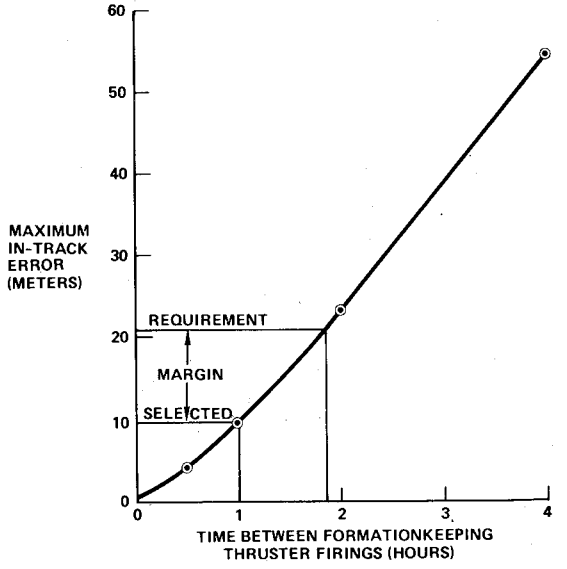

Fig. 13 In-track error vs time interval between thruster firings.

time between in-plane thruster firings for the worst-case case conditions (i.e., equinox, beginning-of-life, sensor noise, and worst-case bias without the predetermined "open-loop" thruster profile). The requirement is that the maximum in-track error be less than 21 m. The selected time interval between in-plane thruster firings is 1 h. The difference represents design margin.

These results show that as the in-plane error requirement is relaxed, the time between thruster firing T can be increased until the Nyquist limit is reached. The upper limit on the time between in-plane corrections is approximately one-third the orbit period.

Conclusions

This paper presented a practical formationkeeping controller consisting of a digital control law, a simple optical sensor, and thrusters on the slave satellite for a pair of satellites in a circular orbit. The control concept is general and could be applied to any of the examples in the introduction.

Simulation results for two geosynchronous satellites with different solar ballistic coefficients and orbiting 700 m apart in trail demonstrated performance which met a ±21 m requirement both in-track and out-of-plane. The accuracy requirement dictates the time between thruster firings. The upper limit for the in-plane digital controller—to avoid aliasing—is one-third the orbit period. The results show that in-plane formationkeeping is more difficult than out-of-plane formationkeeping because of the coupling in the in-plane orbit dynamics and the in-plane solar disturbance at orbit frequency. For equal in-plane and out-of-plane error requirements, in-plane corrections must be applied approximately four times as often as out-of-plane corrections. Adding an open-loop thrust profile to the closed-loop controller further improves performance (results for this case were not shown), since the closed-loop controller is acting on the (smaller) residual error.

Appendix: Derivation of Clohessey-Wiltshire Equations for Two Perturbed Satellites

Write the equations of motion for the slave satellite *s*,

$$\ddot{\vec{r}}_0+\ddot{\vec{\rho}}_s+\frac{\mu}{|\vec{r}_0+\vec{\rho}_s|^3}(\vec{r}_0+\vec{\rho}_s)=\vec{f}_s \tag{A1}$$

Write the equations of motion for the master satellite *m*,

$$\ddot{\vec{r}}_0+\ddot{\vec{\rho}}_m+\frac{\mu}{|\vec{r}_0+\vec{\rho}_m|^3}(\vec{r}_0+\vec{\rho}_m)=\vec{f}_m \tag{A2}$$

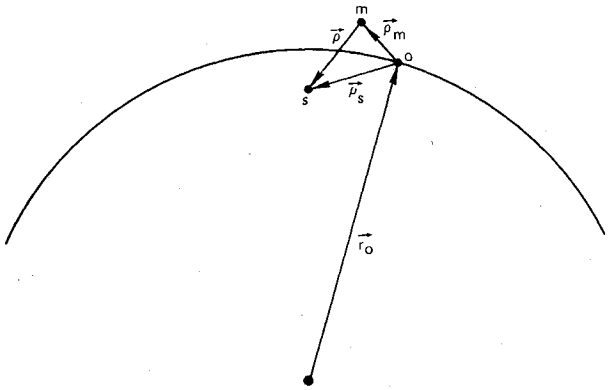

Fig. A1 Relative satellite geometry.

Now obtain the equation of motion of the slave satellite relative to the master by subtracting Eq. (A2) from Eq. (A1) and making the substitution $\vec{\rho}=\vec{\rho}_s-\vec{\rho}_m$,

$$\ddot{\vec{\rho}}+\frac{\mu}{|\vec{r}_0+\vec{\rho}_m+\vec{\rho}|^3}(\vec{r}_0+\vec{\rho}_m+\vec{\rho})-\frac{\mu}{|\vec{r}_0+\vec{\rho}_m|^3}(\vec{r}_0+\vec{\rho}_m)=\vec{f}_s-\vec{f}_m \tag{A3}$$

Expand the denomenators in Eq. (A3) and throw out terms second order or higher in ρ/r_0 or ρ_m/r_0.

$$\frac{1}{|\vec{r}_0+\vec{\rho}_m|^3}=\frac{1}{[(\vec{r}_0+\vec{\rho}_m+\vec{\rho})\cdot(\vec{r}_0+\vec{\rho}_m+\vec{\rho})]^{3/2}}\simeq\frac{1}{r_0^3}\left[1-3\left(\hat{r}_0\cdot\frac{\vec{\rho}_m}{r_0}\right)-3\left(\hat{r}_0\cdot\frac{\vec{\rho}}{r_0}\right)\right] \tag{A4}$$

$$\frac{1}{|\vec{r}_0+\vec{\rho}_m|^3}=\frac{1}{[(\vec{r}_0+\vec{\rho}_m)\cdot(\vec{r}_0+\vec{\rho}_m)]^{3/2}}\simeq\frac{1}{r_0^3}\left[1-3\left(\hat{r}_0\cdot\frac{\vec{\rho}_m}{r_0}\right)\right] \tag{A5}$$

Substitute Eqs. (A4) and (A5) into Eq. (A3),

$$\ddot{\vec{\rho}}+\frac{\mu}{r_0^2}\left(\hat{r}_0+\frac{\vec{\rho}_m}{r_0}+\frac{\vec{\rho}}{r_0}\right)\left[1-3\left(\hat{r}_0\cdot\frac{\vec{\rho}_m}{r_0}\right)-3\left(\hat{r}_0\cdot\frac{\vec{\rho}}{r_0}\right)\right]-\frac{\mu}{r_0^2}\left(\hat{r}_0+\frac{\vec{\rho}_m}{r_0}\right)\left[1-3\left(\hat{r}_0\cdot\frac{\vec{\rho}_m}{r_0}\right)\right]=\vec{f}_s-\vec{f}_m \tag{A6}$$

Multiply, throw out terms second order or higher in ρ/r_0 or ρ_m/r_0, and collect terms. The resulting equation is the general vector form of the Clohessey-Wiltshire equations (note: the second term in the brackets is the gravity gradient term),

$$\ddot{\vec{\rho}}+\frac{\mu}{r_0^3}[\vec{\rho}-3(\hat{r}_0\cdot\vec{\rho})\hat{r}_0]=\vec{f}_s-\vec{f}_m \tag{A7}$$

The scalar form of the Clohessey-Whitshire equations are obtained by making the following substitutions in Eq. (A7) (coordinate frame is shown in Fig. A1),

$$\vec{\rho}=\begin{bmatrix}x\\y\\z\end{bmatrix},\quad\ddot{\vec{\rho}}=\begin{bmatrix}\ddot{x}-2\omega_0\dot{z}-\omega_0^2x\\\ddot{y}\\\ddot{z}+2\omega_0\dot{x}-\omega_0^2z\end{bmatrix},\quad\frac{\mu}{r_0^2}=\omega_0^2,$$

$$\hat{r}_0=\begin{bmatrix}0\\0\\-1\end{bmatrix},\quad\vec{f}_s-\vec{f}_m=\vec{f}=\begin{bmatrix}f_x\\f_y\\f_z\end{bmatrix}$$

Collecting terms we obtain linearized equations that describe the motion of the slave satellite relative to the master

$$\ddot{x}-2\omega_0\dot{z}=f_x$$

$$\ddot{y}+\omega_0^2y=f_y$$

$$\ddot{z}+2\omega_0\dot{x}-3\omega_0^2z=f_z \tag{A8}$$

References

[1]"Shuttle 7 to Fly Approaches to Payload," *Aviation Week and Space Technology,* Vol. 118, No. 19, May 9, 1983, pp. 51-57.

[2]Seifert, H.S. (ed.), *Space Technology,* John Wiley & Sons, New York, 1959, pp. 26.28-26.32.

[3]Clohessy, W.H. and Wiltshire, R.S., "Terminal Guidance System for Satellite Rendezvous," *Journal of the Aerospace Sciences,* Vol. 27, No. 9, Sept. 1960, pp. 653-658, 674.

[4]Lange, B., "The Control and Use of Drag-Free Satellites," Ph.D. Thesis, Dept. of Aeronautics and Astronautics, Stanford University, Stanford, Calif., SUDAAR No. 194, June 1964, pp. 115-125.

[5]Bryson, A.E., *Stabilization and Control of Flight Vehicles,* Draft of 4/1/81, pp. 5.3 (p. 1) through 5.5 (p. 4).

[6]Bryson, A.E. and Ho., Y.-C., *Applied Optimal Control,* rev. ed., John Wiley & Sons, New York, 1975, pp. 428-429.

[7]Kwakernaak, H. and Sivan, R., *Linear Optimal Control Systems,* John Wiley & Sons, New York, 1972, pp. 490-501.

[8]Franklin, G.F. and Powell, J.D., *Digital Control of Dynamic Systems,* Addison-Wesley Publishing Co., Reading Mass., 1980, pp. 251-259.

[9]Katz, P., *Digital Control Using Microprocessors,* Prentice-Hall, Englewood Cliffs, N.J., 1981, pp. 270-277.